Shaping the chameleon

Jonathan A. Pearson*

School of Physics & Astronomy
University of Nottingham
Nottingham, NG7 2RD

October 24, 2014

Abstract

In conservation with Clare Burrage, Ed Copeland, James Stevenson, Adam Moss...

Contents

*E-mail: j.pearson@nottingham.ac.uk

1 Introduction

The idea is to understand the differences between the chameleon force and gravitational force for source objects with different shapes – circles, ellipsoids, etc.

The aim is to build on the analytic results and understanding developed by Burrage, Copeland, and Stevenson; they developed analytic solutions to the governing equations whilst using some simplifying (and justified) assumptions about the dominant contributions to the relevant equations. They obtained the fields surrounding an ellipsoid source. We intend to reproduce their results, and extend to other shapes. This necessitates the use of numerical methods.

2 The model

In the static regime the chameleon scalar ϕ satisfies

$$\nabla^2\phi = -\frac{\Lambda^5}{\phi^2} + \frac{\rho}{M}, \tag{2.1a}$$

and the gravitational potential Φ satisfies Laplace's equation,

$$\nabla^2\Phi = -\rho \tag{2.1b}$$

The forces due to the chameleon and gravitational scalars are computed by taking the gradient of the relevant scalar:

$$\mathbf{F}_{(\phi)} = -\nabla\phi, \qquad \mathbf{F}_{(\Phi)} = -\nabla\Phi. \tag{2.2}$$

We solve (2.1a) using numerical methods outlined in Appendix A for a given source density function, $\rho(\mathbf{x})$.

2.1 Specification of the source density profile

We use a "step-function" to describe ρ, whereby the density has value ρ_0 in the interior of the source, and ρ_{bg} in the exterior of the source (this is supposed to represent the ambient, possibly cosmological, density). To be concrete, we set

$$\rho(\mathbf{x}) = \begin{cases} \rho_0 & \text{inside,} \\ \rho_{\text{bg}} & \text{outside.} \end{cases} \tag{2.3}$$

The spatial locations which are defined as "inside" and "outside" are those inside the given shape under consideration (circles, ellipses, etc).

2.2 Boundary conditions and parameter values

For boundary conditions we set

$$\phi(\mathbf{x}_\infty) = \phi_{\rm bg} = \sqrt{\frac{M\Lambda^5}{\rho_{\rm bg}}}\,. \tag{2.4}$$

This is the value of the scalar which minimizes the effective potential.

Typically we set

$$\Lambda = 1, \qquad M = 10^3, \qquad \rho_0 = 12, \qquad \rho_{\rm bg} = 0.1. \tag{2.5}$$

This is the hierarchy of scales required to obtain the screening solutions of interest. Note that we require a large density contrast, $\delta \equiv \frac{\rho_0}{\rho_{\rm bg}} - 1$, and large M.

3 Results in 2D

Here we present results of numerically solving the equations in 2D; the chameleon scalar ϕ satisfies

$$\frac{\partial^2\phi}{\partial x^2} + \frac{\partial^2\phi}{\partial y^2} = -\frac{\Lambda^5}{\phi^2} + \frac{\rho(x,y)}{M}. \tag{3.1}$$

3.1 Circular sources

Here we define the shape to be inside the circle

$$x^2 + y^2 = R^2. \tag{3.2}$$

See Figure 1 for a plot of the chameleon force; there is a shell of "force" around the object. The force increases linearly inside the object, and then dies off with some negative power in the exterior. In Figure 2 we provide some more illuminating plots, showing the gravitational potential, and the forces generated by the circular source. One may be nervous about the form of the gravitational force: it increases with distance from the source. This corresponds exactly to the behavior we found from the analytic solution, which we plotted in Figure 6 in Appendix B (this is, in some sense, a feature which is present due to the non-zero background density).

3.2 Ellipsoidal sources

Here we define the shape to be inside the ellipse

$$\left(\frac{x}{b}\right)^2 + \left(\frac{y}{a}\right)^2 = R^2 \tag{3.3}$$

See Figure 3 for a plot of the chameleon force density, and Figure 4 for comparisons of the gravitational and chameleon forces down the x- and y-axes.

3.3 Other shapes

Figure 5.

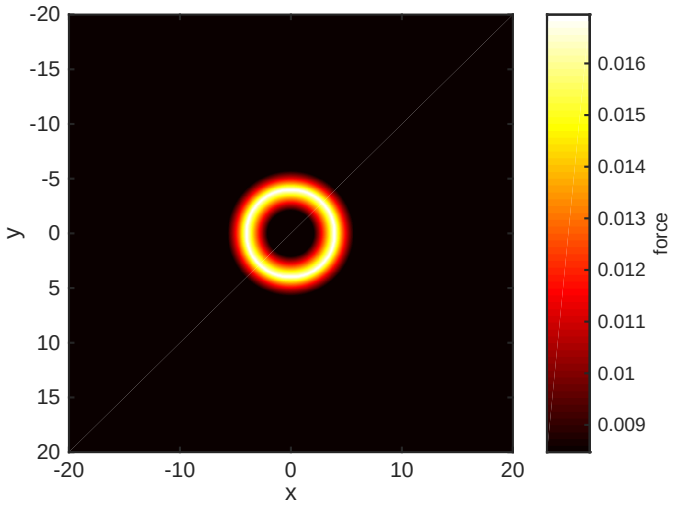

Figure 1: The force density due to the chameleon around a circular source. This source has size $R = 4$. The other parameter values are those given in (2.5). The colour scheme is such that the largest forces are the brightest colours, and any forces lower than half of the maximum are coloured in black. The force increases linearly from the origin, until some maximum is reached at the objects surface; this is better shown in Figure 2(c).

4 Using the *cartoon* method to shape chameleons in 3D

The codes used in Section 3 use gradient flow to obtain the shape of the chameleon fields in 2D. This is an initial choice, born out of numerical simplicity (as well as being able to easily see everything that is going on). However, as discussed in Appendix B, the gravitational potential in 2D and 3D are rather different in nature: and so we want to be able to test whether force discrepancies in 2D are due to the chameleon, or because we are using 2D.

It is now to be remarked that whilst the numerical algorithms are simple to extend from 2D to 3D, the increase in computational resources is substantial. We can make progress if we assume that the source in 3D is axially symmetric. This allows us to obtain the chameleon profiles in a 2D slice of the object: this slice must be rotated forwards and backwards to capture the 3D-ness. One can also impose some periodic breaking of axial symmetry. This is the essence of the *cartoon* method [1].

The idea is to perform gradient flow in Cartesian coordinates in the $(x, y, z) = (x, 0, z)$-plane, and then extrapolate the fields into the $y = \pm\Delta x$ planes using the assumed axial symmetry. This strategy has been sucessfully used in the construction of axially symmetric solitons, specifically cosmic vortons [2].

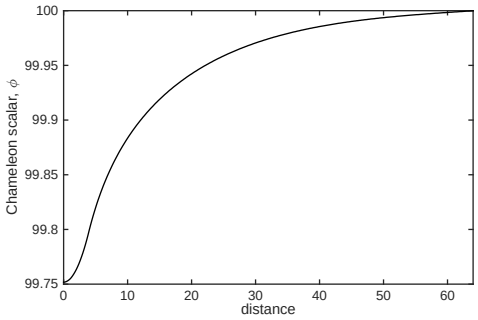

(a) Chameleon scalar

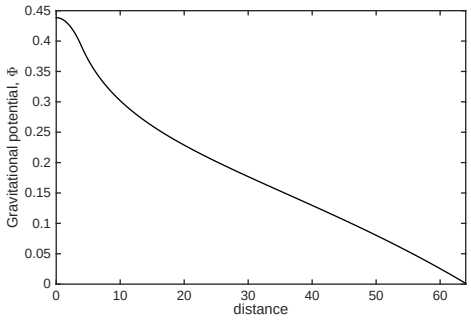

(b) Gravitational potential

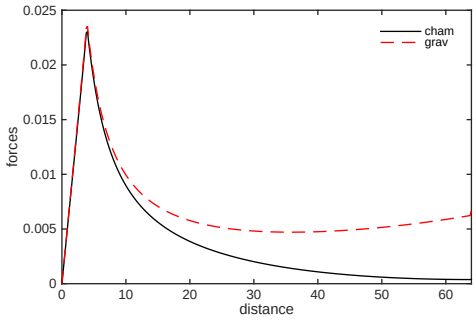

(c) Gravitational and chameleon forces

Figure 2: Plots of various fields for the same 2D circular source as given in Figure 1. In (a) and (b) we plot the values of the chameleon scalar and gravitational potential as a function of distance from the centre of the circular source. One should note that the value of $\Phi(0)$ is arbitrary, since Poisson's equation is invariant under the shift $\Phi \to \Phi + c$, where c is a constant. In (c) we plot the forces due to the gravitational and chameleon scalars.

5 Discussion

Acknowledgements

A Numerical methods

In summary, our numerical methodology is:

- Solve for the chameleon scalar (2.1a) via gradient flow; finite difference derivatives discretized to fourth order accuracy.
- Solve Poisson's equation (2.1b) via SoR; discretized to second order accuracy.
- The forces (2.2) are computed with finite difference derivatives discretized to fourth order

In the remainder of this Appendix we shall explain the implementation of each of these methods.

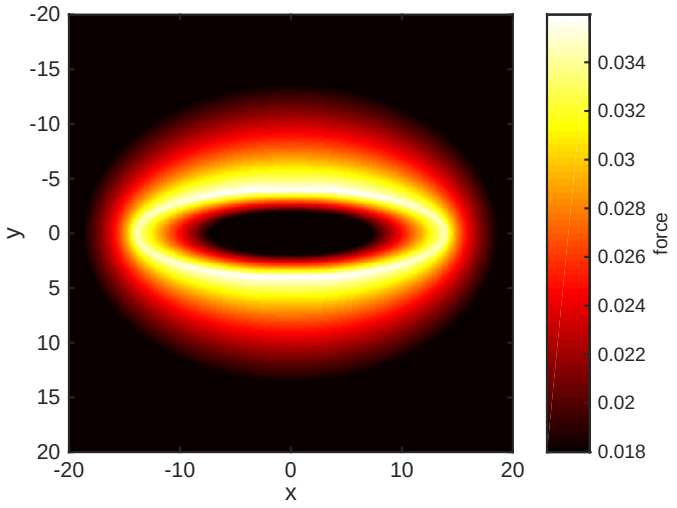

Figure 3: Force due to the chameleon around an ellipsoidal source. This source has $a = 3.5, b = 1$, *and* $R = 4$ *as defined in (3.3); the densities and all other parameters are the same as the source shown in Figure 1. Here we observe that the force profiles along the* x- *and* y-*axes are rather different. The force at the object's surface at* $y = 0$ *is lower than the force at the object's surface at* $x = 0$.

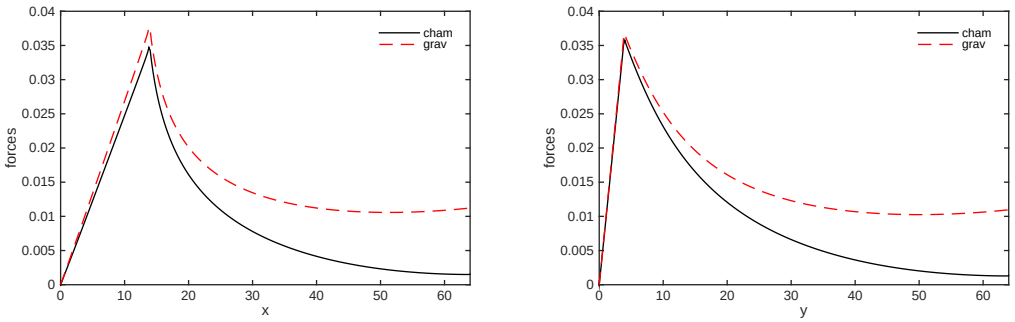

(a) Down the x-axis

(b) Down the y-axis

Figure 4: Comparisons of the chameleon and gravitational forces down the x- *and* y-*axes for the elliptical source shown in Figure 3. The maximum force acheived at the source's surface is largest down the* y-*axis for the chameleon force, and down the* x-*axis for the gravitational force. This is only very slight for the example shown here, but highlights an important distinction between the nature of the gravitational and chameleonic forces (this also corroborates one of the main results of Stevenson et al).*

A.1 Gradient flow

The scalar field profile is obtained by solving the gradient flow equation:

$$\dot{\phi} = \nabla^2\phi - \frac{\mathrm{d}V_{\text{eff}}}{\mathrm{d}\phi}. \tag{A.1}$$

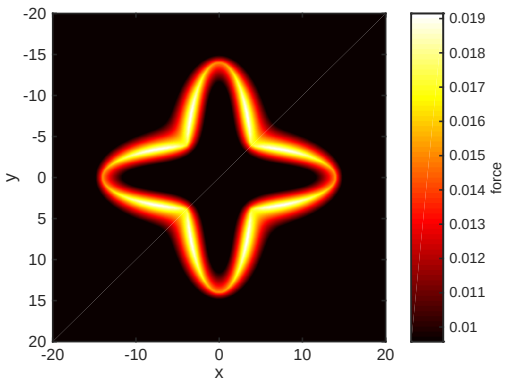

(a) Crossed ellipses

Figure 5: The force due to the chameleon around various sources. In (a) there are two ellipses at right-angles each with the same properties as those in Figure 3. [replace with converged versions]

We discretize the time derivative in a very simple manner,

$$\dot{\phi} \approx \frac{\phi(t+1) - \phi(t)}{h_t}. \tag{A.2}$$

This can be used on the LHS of (A.1) to yield an updating algorithm for the scalar; obviously, we also need a scheme to approximate the Laplacian: that is discussed in the next section. Note that we use a "fictitious time-step", h_t: this must be chosen to be much smaller than any step-sizes in the spatial dimensions (else the problem is badly defined numerically).

A "solution" to the static problem is obtained when $\dot{\phi} = 0$. This is quantified by computing an error estimate

$$E_\phi \equiv \int \mathrm{d}^2x\, \dot{\phi}, \tag{A.3}$$

and waiting until $E_\phi \ll \varepsilon$, where ϵ is supposed to be a very small number, before a solution is declared to have been found. We are also estimating the error on a solution by computing the evolution of the integral of the modulus of the force,

$$E^{\mathrm{F}}_\phi \equiv \int \mathrm{d}^2x\, \left|\mathbf{F}_{(\phi)}\right|; \tag{A.4}$$

this quantity should be independant of time, and so we wait until $\dot{E}^{\mathrm{F}}_\phi \ll \varepsilon$ before declaring that a solution has been found.

A.2 Discretization schemes

Here we explain the discretization schemes used. Space is discretized onto a lattice with step-size h.

A.2.1 Fourth order finite difference derivatives

The first and second derivatives of a quantity Q, say, are approximated at a given location via a fourth-order accurate finite difference scheme according to

$$\frac{\partial Q}{\partial x} \approx \frac{-Q_{i+2} + 8Q_{i+1} - 8Q_{i-1} + Q_{i-2}}{12h}, \tag{A.5}$$

$$\frac{\partial^2 Q}{\partial x^2} \approx \frac{-Q_{i+2} + 16Q_{i+1} - 30Q_i + 16Q_{i-1} - Q_{i-2}}{12h^2}. \tag{A.6}$$

There are obvious equivalents for the y-derivatives.

A.2.2 SoR

This is used to solve Laplace's equation. Fictitious "time-steps" are used, and indexed by n. Convergence is determined by the parameter ω. The updating algorithm is

$$Q^{n+1}_{i,j} = (1-\omega)Q^n_{i,j} + \frac{\omega}{4}\left[Q^n_{i+1,j} + Q^{n+1}_{i-1,j} + Q^n_{i,j+1} + Q^{n+1}_{i,j-1} + h^2\rho\right] \tag{A.7}$$

A.3 Simulated annealing

We have a suggestion to obtain the optimal shape via simulated annealing. This would be implemented by first specifying some given matter distribution (e.g., a sphere), and computing the scalar and gravitational forces. A new shape is randomly proposed – by switching "on" or "off" locations which are supposed to have matter. If the force discrepancies are greater for this new shape, it is kept, and the whole process is repeated until an optimal shape is obtained. One needs to be careful to only proposed connected objects.

This strategy is relatively straight-forward, but computationally very intensive – one way to help is to parallelise the code.

B Solving Poisson's equation for symmetric sources

Here we solve Poisson's equation,

$$\nabla^2\Phi = -\rho/M, \tag{B.1}$$

for a source with constant density ρ_0 immersed in a medium with density $\rho_{\rm bg}$; the source has radius R.

B.1 Poisson's equation in 2D

Here we assume a 2D circular source. Due to the symmetry of the source, the gravitational potential $\Phi = \Phi(r)$ only. Note that the Laplacian in 2D polars is

$$\nabla^2\Phi = \frac{1}{r}\frac{\mathrm{d}}{\mathrm{d}r}\left(r\frac{\mathrm{d}\Phi}{\mathrm{d}r}\right). \tag{B.2}$$

The solution is

$$\Phi(r) = -\frac{\rho}{4M}r^2 + A\ln r + B, \tag{B.3}$$

where A and B are integration constants; their values will be fixed by requiring continuity, smoothness, and regularity in various regimes. The radial component of the force (the only component, infact) is

$$F_r(r) = \frac{\rho}{2M}r - \frac{A}{r}. \tag{B.4}$$

From hereon we will drop the "r" index from the force component. We are interested in obtaining the gravitational potential surrounding and within a circle of radius R, density ρ_0, immersed in a background density $\rho_{\rm bg}$. One requires $A_{\rm in} = 0$ for regularity at the origin. By matching the forces at the surface $r = R$ one obtains the expression for $A_{\rm out}$,

$$A_{\rm out} = \frac{\rho_{\rm bg}R^2}{2M}\left(1 - \frac{\rho_0}{\rho_{\rm bg}}\right). \tag{B.5a}$$

By matching the potentials, one also obtains

$$B_{\rm bg} = B_0 + \frac{R^2\rho_{\rm bg}}{4M}\left(1 - \frac{\rho_0}{\rho_{\rm bg}}\right)(1 - 2\ln R). \tag{B.5b}$$

The potential inside and outside the object is given by

$$\Phi_{\rm in}(r) = -\frac{\rho_0}{4M}r^2 + B_0, \tag{B.6a}$$

$$\Phi_{\rm out}(r) = -\frac{\rho_{\rm bg}}{4M}r^2 + \frac{\rho_{\rm bg}R^2}{2M}\left(1 - \tfrac{\rho_0}{\rho_{\rm bg}}\right)\ln r + B_0 + \frac{R^2\rho_{\rm bg}}{4M}\left(1 - \tfrac{\rho_0}{\rho_{\rm bg}}\right)(1 - 2\ln R), \tag{B.6b}$$

and the force inside and outside are given by

$$F_{\rm in}(r) = \frac{\rho_0}{2M}r, \tag{B.7a}$$

$$F_{\rm out}(r) = \frac{\rho_{\rm bg}}{2M}r - \frac{\rho_{\rm bg}R^2}{2M}\left(1 - \tfrac{\rho_0}{\rho_{\rm bg}}\right)\frac{1}{r}. \tag{B.7b}$$

See Figure 6 for a plot of these solutions.

B.2 Poisson's equation in 3D

In 3D, for a spherically symmetric gravitational potential, the Laplacian reads

$$\nabla^2\Phi = \frac{1}{r^2}\frac{\mathrm{d}}{\mathrm{d}r}\left(r^2\frac{\mathrm{d}\Phi}{\mathrm{d}r}\right). \tag{B.8}$$

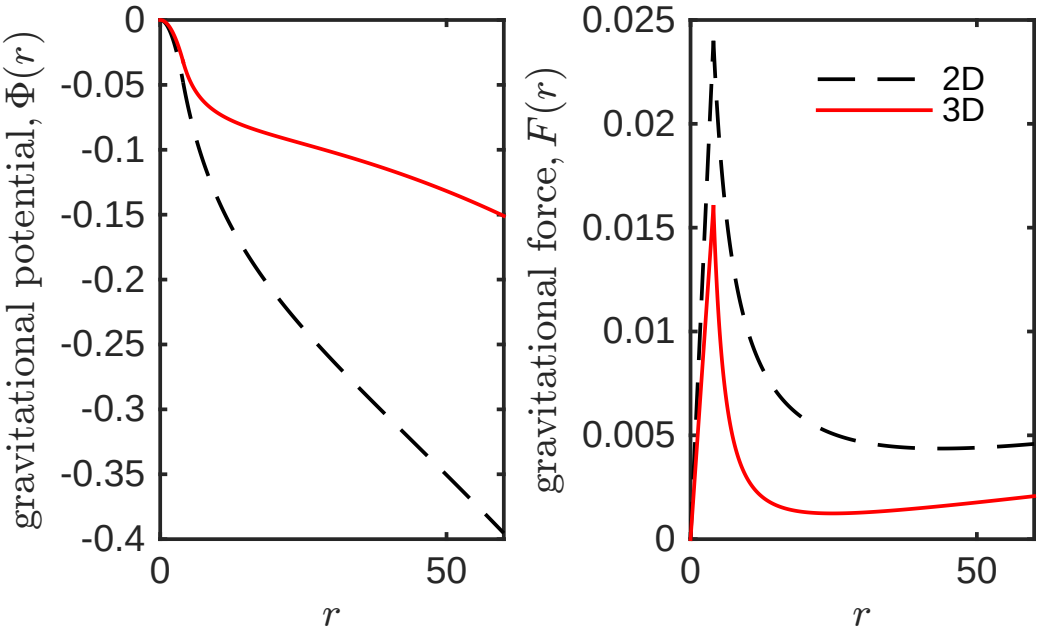

Figure 6: The gravitational potential (left) and force (right) for 2D and 3D circularly and spherically symmetric sources with constant density. These correspond to the solutions we presented in Appendix B. The values of the parameters are exactly those we gave in (2.5), along with $R = 4$ for the radius of the source.

The solution to Poisson's equation (again, with a constant source density ρ) is

$$\Phi(r) = -\frac{\rho}{6M} r^2 - \frac{A}{r} + B, \tag{B.9}$$

in terms of two integration constants A and B. After requiring continuity and regularity, the potential and force inside and out are given by

$$\Phi_{\text{in}}(r) = -\frac{\rho_{\text{in}}}{6M} r^2 + B_{\text{in}}, \tag{B.10a}$$

$$\Phi_{\text{out}}(r) = -\frac{\rho_{\text{out}}}{6M} r^2 + \frac{\rho_{\text{out}} R^3}{3M} \left(\tfrac{\rho_{\text{in}}}{\rho_{\text{out}}} - 1 \right) \frac{1}{r} + \frac{\rho_{\text{out}} R^2}{2M} \left(1 - \tfrac{\rho_{\text{in}}}{\rho_{\text{out}}} \right) + B_{\text{in}}, \tag{B.10b}$$

$$F_{\text{in}}(r) = \frac{\rho_{\text{in}}}{3M} r, \tag{B.11a}$$

$$F_{\text{out}}(r) = \frac{\rho_{\text{out}}}{3M} r + \frac{\rho_{\text{out}} R^3}{3M} \left(\tfrac{\rho_{\text{in}}}{\rho_{\text{out}}} - 1 \right) \frac{1}{r^2}. \tag{B.11b}$$

See Figure 6 for a plot of these solutions.

References

[1] M. Alcubierre, S. Brandt, B. Bruegmann, D. Holz, E. Seidel, *et. al.*, *Symmetry without symmetry: Numerical simulation of axisymmetric systems using Cartesian grids*, *Int.J.Mod.Phys.* **D10** (2001) 273–290, [gr-qc/9908012].

[2] R. A. Battye and P. M. Sutcliffe, *Vorton construction and dynamics*, *Nucl.Phys.* **B814** (2009) 180–194, [arXiv:0812.3239].